HOSTED BY
ELSEVIER
Available online at www.sciencedirect.com
ScienceDirect
Soils and Foundations 63 (2023) 101376
www.elsevier.com/locate/sandf

Technical Note

A simple continuum approach to predict the drained pull-out response of piles for offshore wind turbines

Riccardo Zabatta [a,1], Laura Govoni [a], Aligi Foglia [b,2], Alessio Mentani [a,*]

[a] DICAM, University of Bologna, Bologna, Italy
[b] Norwegian Geotechnical Institute, Oslo, Norway

Received 8 November 2022; received in revised form 3 August 2023; accepted 3 September 2023
Available online 27 September 2023

Abstract

The article presents a continuum approach to predict the response of pile foundations for jacket-supported offshore wind turbines. Tensile loading conditions are examined, which may be critical for piles used in combination with this structure type, generally adopted to exploit wind energy in intermediate water depths. The approach is developed to guarantee a simple implementation with a limited number of input data easily attainable from cone penetration tests and laboratory tests, and to ensure computational cost-effectiveness. Data from technical-scale tests on open-ended steel piles driven in dense sand and subjected to drained pull-out are used to assess the performance of the approach. The results are shown to be accurate, approximating rather closely the experimental load–displacement curves. The accuracy of the approach is also compared to that obtained with a recently proposed design method, to investigate the predictive capacity of the approach and its potential to support preliminary design activities.

Keywords: Single driven piles; Sand; Finite Element Modelling (FEM); Cone Penetration Test (CPT); Soil-structure interaction

1. Introduction

Jacket platforms on driven piles are commonly employed structural solutions to exploit offshore wind in intermediate water depths. In this configuration, the foundations are prevalently subjected to axial loads, which may become onerous in tension, due to the light weight of the superstructure.

The response to pull-out of pile foundations is traditionally estimated using the load-transfer curve approach, combined with ultimate shaft friction prediction methods. For offshore piles, the ultimate shaft friction is currently estimated using Cone Penetration Test-based procedures (CPT methods). These methods were developed over the last two decades using a wide experimental database and recently collected under a unified formulation (Lehane et al., 2020a). The pile response prior to failure depends on the choice of the load-transfer formulation. Different approaches were lately shown to yield good results when applied to offshore piles (e.g. Zhang et al., 2019, Lehane et al., 2020b) but, unlike for the pile capacity prediction methods, there is no common agreement on which one is to be favoured.

To address this specific loading condition, less attention has been generally given to continuum approaches (De Nicola and Randolph, 1993; Broere and Van Tol, 2006) which are instead extensively employed for combined and lateral loading (e.g. Wakai et al., 1999; Hu et al., 2022).

In general, a reliable modelling approach should be able to adequately mimic the effects of pile installation, includ-

* Corresponding author.
E-mail addresses: riccardo.zabatta2@unibo.it (R. Zabatta), l.govoni@unibo.it (L. Govoni), aligi.foglia@ngi.no (A. Foglia), alessio.mentani2@unibo.it (A. Mentani).
[1] Formerly DICAM, University of Bologna, Bologna, Italy.
[2] Formerly Fraunhofer IWES, Hannover, Germany.

https://doi.org/10.1016/j.sandf.2023.101376
0038-0806/

Nomenclature

D	pile diameter	γ_{soil}	unit weight of the surrounding soil
L	pile length	K_E	Young's modulus number
t	pile thickness	p'_{0i}	post-installation mean effective stress
D_i	inner diameter of the pile	I_{cn}	normalised soil behaviour type index
D_r	soil relative density	G_{adj}	shear modulus of the adjacent soil
q_c	cone tip resistance	G^*	model constant
$q_{c,art}$	artificial cone tip resistance	s_{adj}	thickness of the adjacent soil
p_a	atmospheric pressure (=100 kPa)	D_{50}	mean particle size of the sand
p'_0	mean effective stress at rest	δ_{yield}	model constant and yield interface friction angle
σ'_{v0}	vertical effective stress at rest	δ_{cv}	constant volume interface friction angle
σ'_{ri}	post-installation radial stress	b	model constant
σ'_{θ}	circumferential stress	γ^p	plastic shear strain
PLR	pile Plug Length Ratio	ψ_{adj}	dilation angle of the adjacent soil
h	distance of the local depth to the pile head	e_{min}	minimum void ratio of the material
$\phi'_{p,soil}$	peak friction angle of the surrounding soil	e_{max}	maximum void ratio of the material
ψ_{soil}	dilation angle of the surrounding soil	ϕ'_{cv}	constant volume friction angle
E_{pile}	Young's modulus of the equivalent pile	R_a	shaft surface average roughness
E_{soil}	Young's modulus of the surrounding soil	R_n	normalised average roughness
v_{pile}	Poisson's ratio of the equivalent pile	V_{ult}	pile tensile capacity prior to failure
v_{soil}	Poisson's ratio of the surrounding soil	w_{ult}	pile head displacement at failure
γ_{pile}	unit weight of the equivalent pile	w'	pile head displacement at service conditions

ing geometrical effects and friction fatigue on the subsequent load stages (Jardine et al., 1998; White and Lehane, 2004) and to correctly model the steel-sand interface behaviour (DeJong et al., 2006). From the standpoint of a realistic model, this implies the use of large-deformation analyses of pile installation to provide the initial stress and state variables (e.g. Heins and Grabe, 2017) within small-strain simulations, performed with advanced interface models (e.g. Staubach et al., 2022). This procedure, however, is still too laborious and computationally onerous for the exploitation in the engineering practice.

The approach presented in the paper lies halfway between one-dimensional approaches which implement load-transfer curves and a realistic modelling procedure. Of the Finite Element (FE) type, it makes use of CPT and interface tests data. The implementation is kept simple and the computational cost low, enabling for parametric studies to be performed, which can be interpreted within the framework of new probabilistic approaches (e.g. Mentani et al., 2022, Mentani et al., 2023). The performance of the approach is evaluated in reproducing technical-scale tests and is compared with recently developed predictive methods.

2. Details of the approach

2.1. Description

The approach addresses the axisymmetric problem of a pile of diameter D, length L and thickness t, driven in a homogeneous deposit of constant relative density, D_r and subjected to a vertical upward displacement, w, at the head (Fig. 1a) in fully drained conditions.

The study assumes that, at the end of the installation phase, the length of the soil plug is equal to that of the pile embedment depth. This installation mode is called cored and is characterised by a Plug Length Ratio, PLR, equal to 1. It is also assumed that, during loading the soil plug perfectly sticks to the inner pile surface. This condition is called fully plugged. Under this circumstance, the pile is pulled out with no relative movement of the inner soil and behaves as it was closed-ended. Such behaviour, cored in installation and fully plugged in loading, is typical of offshore piles (see for instance Randolph and Gourvenec, 2011). According to these hypotheses a uniform cross section is assigned to the pile, of properties suitably averaged to account for the soil and steel components.

The pile is modelled as it was wished in place and the post-installation radial stress in the vicinity of the pile is linked to the local cone tip profile by using empirical correlations available in the literature. This is meant to approximate the effects of pile driving on the soil stress state prior to loading. Recent numerical research findings have showed that the circumferential stress component is also affected by the installation process to an extent that is similar to that observed on the radial (Ciantia et al. 2019). Based on this, and to avoid equilibrium issues in the geostatic step, the same value is prescribed to the radial and circumferential initial stress.

The approach is based on the modelling of three main features: the pile, the soil adjacent to pile shaft and the soil not in contact with the pile wall, and referred hereinafter as

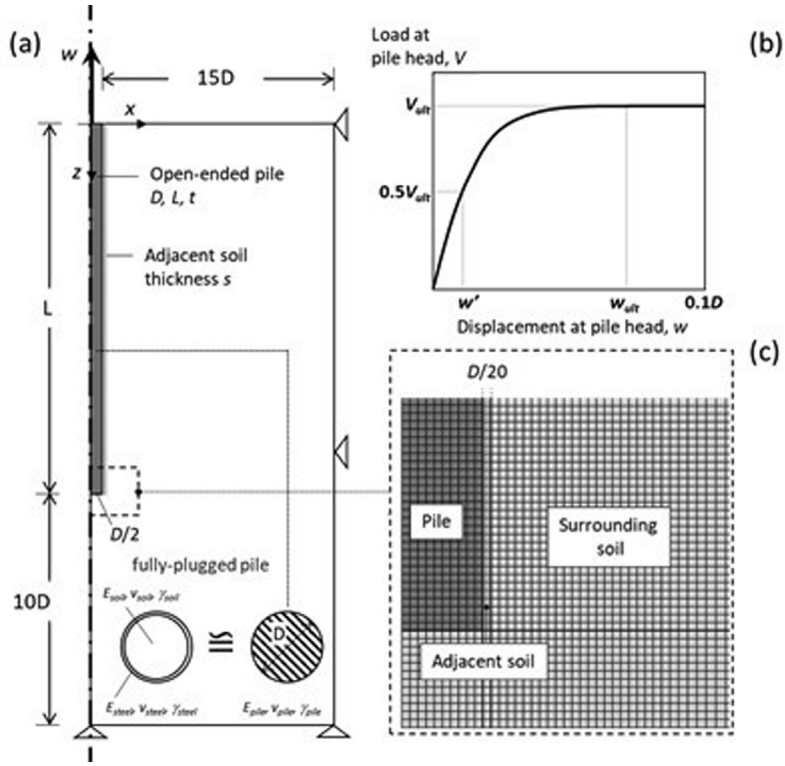

Fig. 1. Schematic overview of the approach: a) geometry, b) expected prediction and c) model mesh adjacent to the pile.

the surrounding soil (Fig. 1c). It is assumed that the shear stress along the pile shaft is mobilised in the adjacent soil, rather than at the interface, to which a rigid response is prescribed up to a failure threshold, governed by the Coulomb failure criterion. The adjacent soil remains attached to the shaft until failure (sticking condition), then, when the failure surface is attained, relative motion can take place (slipping condition). The same resistance is assigned to the interface and to the adjacent soil.

2.2. Implementation

The FE software Abaqus (ABAQUS, 2014) is used to implement the approach. Other commercial packages can be used, as long as they allow for a structured mesh in the vicinity of the pile. Four nodes, bilinear and axisymmetric elements were used. Zero displacement boundaries are set at a 15D distance from the pile shaft and 10D down the pile tip. Details of modelling of the part is given in the following.

2.2.1. Pile

The pile is deformable and obeys to a linear elastic constitutive law, whose constants (E_{pile}, υ_{pile}) and physical properties (γ_{pile}) are averaged accounting for the steel and soil properties and pile thickness.

2.2.2. Surrounding soil

A uniform mesh is assigned up to a distance D to the pile wall, with element thickness set to $D/12$. No effects of further refining the mesh size on the model results were observed. A portion of the model mesh in the vicinity of the pile tip is shown in Fig. 1c.

The linear Drucker Prager (DP) model was assigned to the soil elements employing the linear-elastic, perfectly-plastic formulation. The procedure adopted to identify the model constants is detailed in Table 1, and requires the use of CPT data. These were selected as suitable to clean, medium dense silica sands and steel displacement piles.

An artificial cone resistance $q_{c,art}$, is calculated according to Jamiolkowski et al. (2003) implementing a constant D_r value:

$$q_{c,art} = 24.94 p_a \left(p'_0/p_a\right)^{0.46} e^{2.96\mu_{Dr}} \tag{1}$$

where p'_0 is the mean effective in situ stress at rest, p_a is the atmospheric pressure and μ_{Dr} is the mean soil density. The profile of $q_{c,art}$ is used to set the initial stress field in the soil according to:

$$\sigma'_{ri} = \sigma'_{\theta} = \frac{q_{c,art}}{44}\left[1 - PLR\left(\frac{D_i}{D}\right)^2\right]^{0.3}\left[\max\left[1, \left(\frac{h}{D}\right)\right]\right]^{-0.4} \tag{2}$$

where $PLR = 1$ (as mobilised in the installation phase), D_i is the inner diameter of the pile, h is the vertical distance of the local depth to the pile tip (Lehane et al., 2020a). The equation is relevant to piles driven in sand and explicitly accounts for friction fatigue and geometrical effects (e.g. Lehane et al., 1993). The peak resistance of the soil surrounding the pile is prescribed to vary with depth according to Kulhawy and Mayne (1990):

Table 1
Summary of the proposed procedure.

Steps	Equations	Input data (test)	FE model constants
1. Set an artificial $q_{c,art}$, function of the soil mean relative density D_r, μ_{Dr}.	Equation (1)	$\mu_{Dr} = 0.74$ (CPTs)	used to derive other model constants
2. Use the calculated $q_{c,art}$ to estimate the post-installation radial stress acting on the pile σ'_r and implement the value as initial σ'_{ri} and σ'_{0i}.	Equation (2)		In situ stress$K = \sigma'_{ri}/\sigma'_{v0}$
3. Use the calculated $q_{c,art}$ to predict the evolution of the soil peak friction angle$\phi'_{p,soil}$ with depth.	Equation (3)	$\phi'_{cv} = 32.5°$ (triaxial tests)	Soil, plastic $\phi'_{p,soil}\psi_{soil} = \phi'_{p,soil} - \phi'_{cv}$
4a. Express the soil Young's modulus, E_{soil}, as a power law of the post-installation mean effective stress p'$_{0i}$	Equation (4)	$\mu_{KE} = 1100$	Soil, elastic
4b. Take a constant K_E corresponding to the mean soil value, μ_{KE}.	Equations (5) and (6)	$m = 0.5$ (CPTs)	E_{soil}, $v = 0.3$
5. Set the interface friction angle equal to the critical δ_{cv}	–	$\delta_{cv} = 25°$ (DS interface)	Interface tan(δ_{cv})
6. Calibrate the model constants of soil adjacent to the pile in simple shear conditions using the results of interface direct shear tests assuming the shear band thickness $s = 5D_{50}$.			
6a. Express the shear modulus G_{adj} as function of the confining stress, σ'_n, and thickness, s_{adj}.	Equation (7)	$G^* = 2.2$ mm^{-1} $n = 1$	Adjacent soil, elastic $v = 0.3$, $E_{adj} = G_{adj}[2(1 + v)]$
6b. Identify the friction angle at yield δ_{yield} and dilation angle ψ_{adj}. Best fit to experiments (see Fig. 3)	–	$\delta_{yield} = 8.5°$; $\psi_{adj} = 0.5°$	Adjacent soil, plastic§ δ_{yield}, ψ_{adj}
6c. Set shear stress as function of mobilised plastic shear strain, γ^p and confining stress, σ'_n up to critical state (with $\delta = \delta_{cv}$)	Equation (9)	$\delta_{cv} = 25°$ $b = 0.04$	Adjacent soil, plastic§ Hardening§ $d = f(\gamma^p)$
7a. In the pile model, pick a line of finite elements of thickness $s_{adj}/D = 0.05$ along the pile shaft.			
7b. Incorporate the shear band model constants calibrated in Step 6 using$\sigma'_n = \sigma'_{ri}$			

§ Constants corresponds to plane strain conditions and require non-associated flow matching to DP (ABAQUS, 2014).

$$\phi'_{p,soil} = 17.6 + 11log\left(q_{c,art}/\left(p_a\sigma'_{v0}\right)^{0.5}\right) \quad (3)$$

where $\phi'_{p,soil}$ is the peak friction angle of the material and σ'_{v0} is the vertical effective stress at rest.

The elastic stiffness, E_{soil}, is prescribed to vary with depth according to:

$$E_{soil} = \mu_{KE}p_a\left(p'_{0i}/p_a\right)^m \quad (4)$$

where μ_{KE} and m are dimensionless models constant, calculated as:

$$\mu_{KE} = mean(E_{CPT}/p_a)\left(p'_{0i}/p_a\right)^{-m} \quad (5)$$

$$E_{CPT} = 0.015(10^{0.55I_{cn}+1.68})(q_c - \sigma'_{v0}) \quad (6)$$

where p'_{0i} is the mean, post-installation, effective stress, I_{cn} and q_c are the experimental normalised soil behaviour type index and cone tip resistance and $m = 0.5$ (Robertson, 2009).

2.2.3. Soil adjacent to the pile

The adjacent soil is modelled using the column of elements next to the pile shaft, of thickness $s_{adj} = 0.05D$. The choice of the value was based on the outcomes of a recent, comprehensive set of steel displacement pile tests that involved medium rough to rough piles in medium dense to dense sand (Tovar-Valencia et al., 2018). The linear DP model is assigned to these elements employing the linear-elastic, hardening-plastic formulation.

The shear elastic modulus G_{adj} is prescribed as function of the normal stress acting on the pile shaft (De Gennaro and Frank, 2002):

$$G_{adj} = G^* \cdot s_{adj} \cdot (\sigma\prime_{ri})^n \quad (7)$$

where σ_{ri} is the radial stress of Eq. (2), G^* and n are model constants.

The shear stress at yield is given by:

$$\tau_{yield} = \sigma\prime_{ri} \cdot tan(\delta_{yield}) \quad (8)$$

where δ_{yield} is the slope of the yield surface of the DP model. The yield surface evolves with mobilised plastic shear strain γ^p up to failure, when the mobilised friction angle equals δ_{cv}, according to the hardening law:

$$\tau = \sigma\prime_{ri} \cdot \left[\frac{tan(\delta_{cv}) - tan(\delta_{yield})}{(b + \gamma^p)}\right]\gamma^p \quad (9)$$

where b is a model constant. The flow rule is non-associated and governed by ψ_{adj}. The six model constants (G^*, b, n, δ_{cv}, δ_{yield}, ψ_{adj}) can be calibrated on the interpretation of constant stress interface tests, as described in Section 2.2.

3. Application of the approach to model large-scale pile tests

3.1. Details of the experiment

The tests were carried out by Fraunhofer IWES at the Test Centre for Support Structures of the Leibniz Univer-

sität of Hannover and are selected as they involved offshore piles for wind turbine jackets driven in a uniform sand deposit. Referring to Schmoor et al. (2018) for more experimental details, a schematic of the testing set-up is given in Fig. 2 and relevant information are summarised in the following.

3.1.1. Materials

The soil is a uniform siliceous sand (D_{50} = 0.36 mm, e_{min} = 0.45 and e_{max} = 0.85), previously characterised with triaxial tests (ϕ'_{cv} = 32.5°). For the testing campaign, two direct shear tests were carried out on dense sand specimens (D_r = 0.74) and steel plates of medium roughness (average roughness R_a = 5 μm). Tests were Constant Normal Load (CNL), with pressures set at 60 kPa and 90 kPa. The mobilised friction angle and vertical displacement against the applied horizontal displacement are shown in Fig. 3.

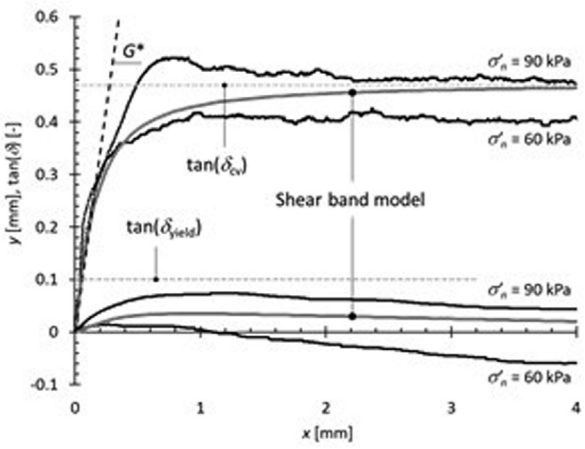

Fig. 3. Identification of the shear band model constants based on the results of interface tests.

3.1.2. Sample preparation

The sample was prepared in the laboratory sand pit to achieve a dense state, overlapping compacted dry sand layers of about 25 cm thickness up to a height of 9.65 m. Saturation was carried out at the end of the process up to 0.5 m below the sample surface. The relative density was measured collecting locally sand specimens and resulted equal to 0.74.

3.1.3. Sample characterisation

Five CPTs were performed at various locations (Fig. 2a). The summary of q_c and sleeve friction is given in Fig. 4. Data fall in a relatively narrow band showing

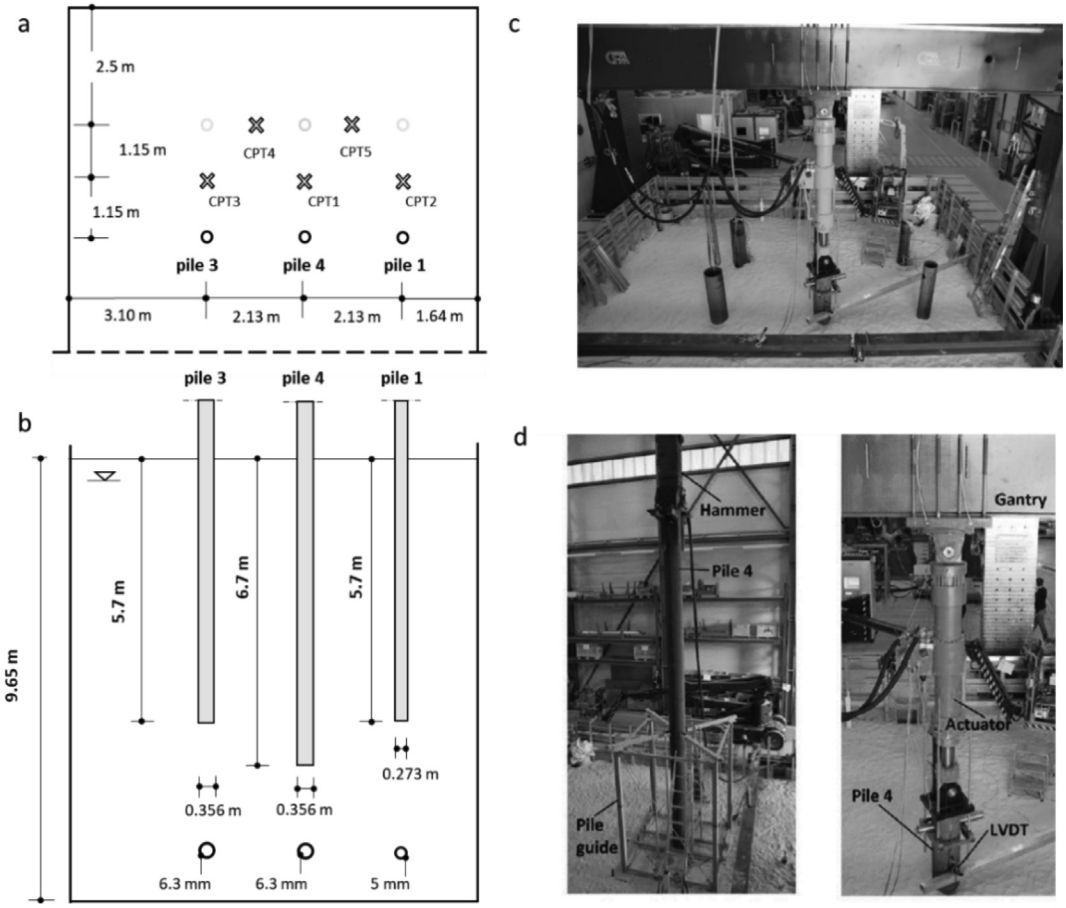

Fig. 2. Schematic drawing of the experimental set-up a) top view, b) section and pics of the piles, c) the pile layout and d) installation and loading.

the tests being consistent with the experimental hypothesis of a homogenous deposit. Fluctuations of constant amplitudes about average values, clearly visible at the tip passage and then attenuated along the shaft, are ascribable to the sample preparation procedure, as already observed in similarly conducted campaign at the same facility (Foglia et al., 2021).

3.1.4. Load tests

The experiments involved three steel, medium rough (average roughness $R_a = 5$ μm) open ended piles (Pile 1, Pile 3 and Pile 4) of dimension given in Table 2, driven using a double-acting pile hammer and subjected to a displacement-controlled pull-out at 0.01 mm/s rate, to ensure drained conditions. The results in terms of normalised vertical displacement and load, in Fig. 5, shows a general good agreement.

3.2. Analyses and results

Employing the available CPT data and laboratory tests, the model constants are identified and the values are inserted in Table 1.

The profile of artificial $q_{c,art}$ (Eq. (1)) is computed using the measured mean sample density $\mu_{Dr} = 0.74$ and shown in Fig. 4a. The value μ_{Dr} compared on the sample density profile, applying again Eq. (1), is instead shown in Fig. 6a, confirming the suitability of the selected empirical

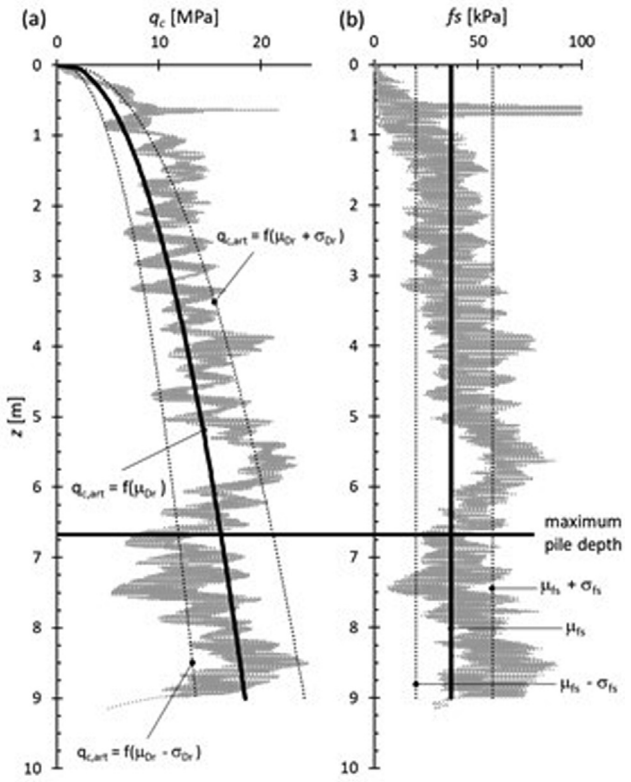

Fig. 4. Summary of CPT results: profiles of a) cone resistance and b) sleeve friction.

Table 2
Details of the model piles used for the application of the modelling procedure.

Test	D [m]	L/D [-]	D/t [-]
Pile 1	0.273	20.9	54.6
Pile 3	0.356	16	56.5
Pile 4	0.356	18.8	56.5

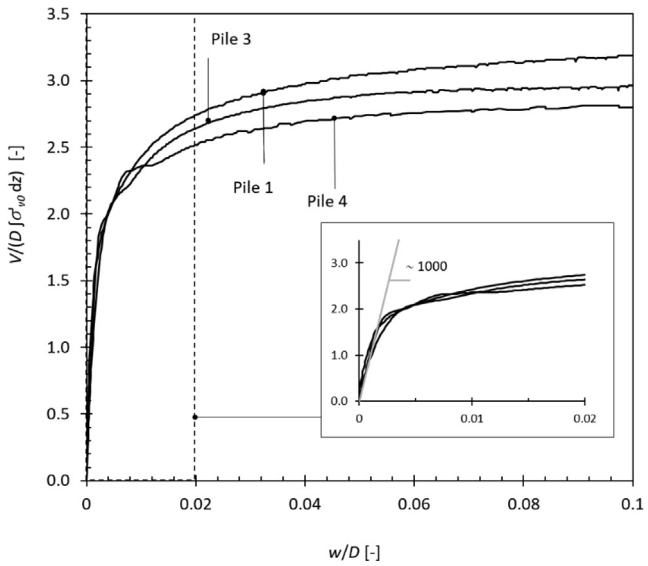

Fig. 5. Experimental normalised load – displacement curves.

correlation for the sand deposit in exam. The value of $q_{c,art}$ is used to calculate the surrounding soil strength (Eq. (3)) and to set the geostatic step according to Eq. (2).

Fig. 6b illustrates the profile of K_E, calculated using Eqs. (5) and (6). The average, $\mu_{KE} = 1100$ (standard deviation, $\sigma_{KE} = 290$), also inserted in Fig. 6b, is used to implement the soil stiffness in the surrounding soil, according to Eq. (4).

The six constants (G^*, n, b, δ_{cv}, δ_{yield}, ψ_{adj}) of the DP model assigned to the adjacent soil elements are calibrated against the available interface tests data. Simple shear, CNL conditions are prescribed to an element of thickness equal to $5D_{50}$, which is a realistic value for shear band heights for medium rough steel plates (e.g. DeJong et al., 2006). The quality of fitting can be observed in Fig. 3, where model and test data are presented along with the identification of the model constants: G^* is the slope of the initial linear branch, while δ_{cv} and δ_{yield}, are the model ultimate and yield interface friction angle respectively. The constant b governs the $\tan(\delta) - x$ curvature, while ψ_{adj} enables to fit the experimentally observed volumetric response.

The FE models of Piles 1, 3 and 4 are created using these inputs. Analyses are small strain, total stress and carried out applying a $0.1D$ upward displacement to the pile head.

The numerical load–displacement curves are compared to the experimental in Fig. 7a, 7b and 7c for Piles 1, 3 and 4, respectively. The three pile models reproduce accu-

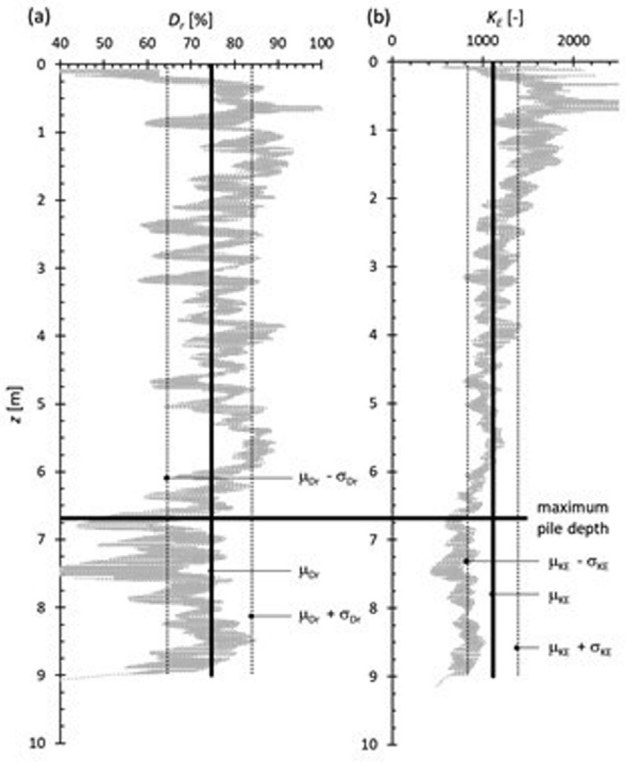

Fig. 6. Identification of the soil model constants a) μ_{Dr} on the experimental D_r profile and b) μ_{KE} on the experimental K_E profile.

rately the entire load displacement response, well capturing the non-linearities prior to failure. Selected values are also identified to assess the performance of the approach. According to Fig. 1b, these are: the mobilised pile head displacement at half of the measured capacity, w', through the normalised parameter $\Delta w' = (w'_{FE} - w'_{Exp})/D$, which shortly describes the service conditions (Lehane et al., 2020b); the tensile capacity, V_{ult}, and the upward pile head displacement at failure, w_{ult}, which instead are representative of the ultimate conditions.

With reference to Δw', the computed values are 0.0024, 0.0010, 0.0014, for Pile 1, 3 and 4, respectively. The agreement is satisfactory and ascribable to the choices made for the surrounding soil modelling. Eq. (4) enables to implement the variation of the stiffness with depth also accounting for the post-installation confining stress, and Eq. (6) is calibrated based on clean silica sand and thus particularly suitable to model the soil used in the experiments. The stiffness remains constant during loading consistent to the generally observed pile response under axial loading (e.g. De Gennaro and Frank, 2002).

The tensile capacity is particularly well predicted, notably for Pile 3 and Pile 4. The 17% underestimation on Pile 1 (Fig. 7a) can be partly ascribable to a comparatively higher experimental normalised capacity (Fig. 5). The available experimental data did not show local inconsistencies at Pile 1, which might have shown possible factors causing this discrepancy to be considered in the FE modelling.

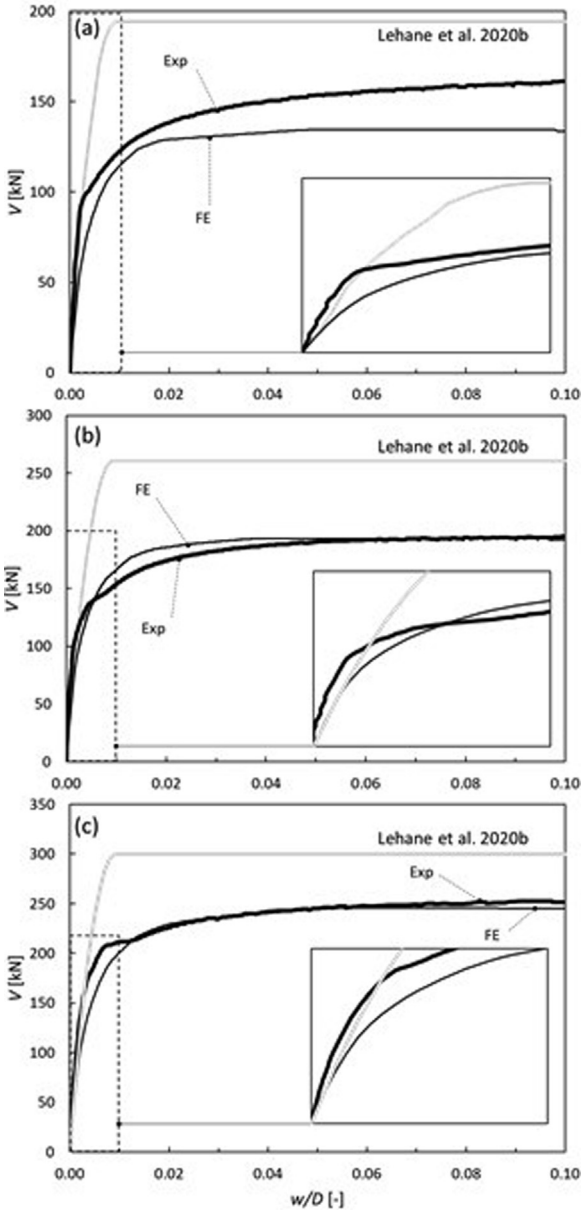

Fig. 7. Comparison of the experimental load–displacement curves with the numerical results of the proposed approach and with the load-transfer curve method from Lehane et al. (2020b) for Pile 1 (a), Pile 3 (b), and Pile 4 (c).

The model evaluates the pile head displacement at failure w_{ult} when all the nodes at the pile-soil interface reach the slipping conditions. The calculated values are $0.05D$, $0.04D$ and $0.06D$ for Pile 1, Pile 3 and Pile 4, respectively. The data compare well with the experimentally observed values, measured on the load–displacement curve when the pile is no longer able to take on additional load. These are equal to $0.06D$ for Pile 3 and $0.07D$ for Pile 4. As Pile 1 still shows to mobilise an increasing resistance to pullout at $w = 0.1D$, the data for comparison could not be inferred. For the ultimate conditions, the agreement could be explained by the implementation of the adjacent soil part, which was calibrated on relevant interface data, notably

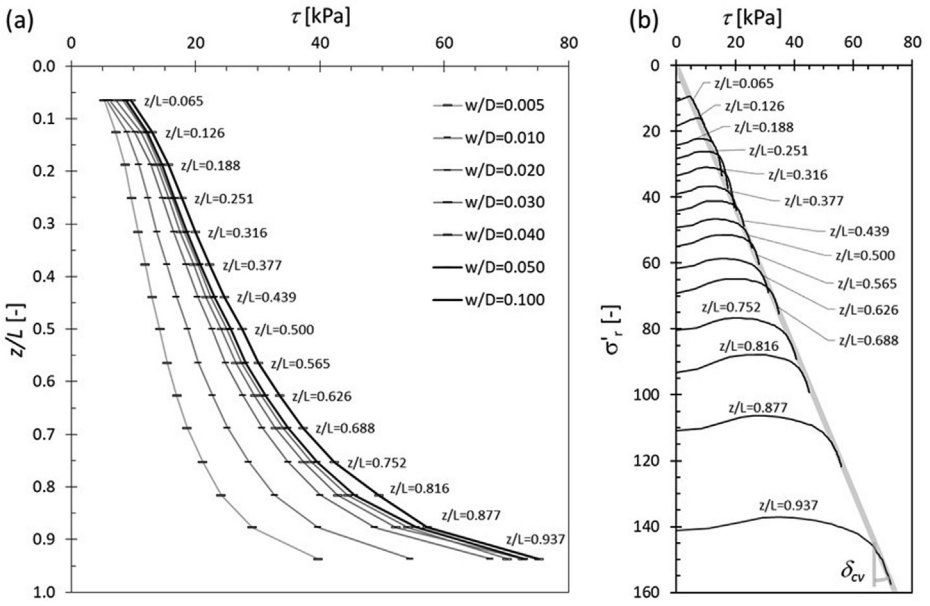

Fig. 8. Shaft resistance mobilisation during loading of Pile 1: (a) evolution of the shear stress mobilisation at the pile shaft during loading; (b) stress paths followed by the elements adjacent to pile towards the failure line.

the δ_{cv}. The implementation of the hyperbolic hardening (Eq. (9)) also allows for the non-linearities prior to failure to be correctly captured, leading to a satisfactory estimation of w_{ult}.

The approach allows to model the progressive mobilisation of the shaft resistance along the pile, as depicted in Fig. 8a, where the non-linear variation during the loading phase ofthe shear stress within the adjacent soil, is shown along with the embedment depth, z/L. In Fig. 8b, the stress paths followed by the elements along the shaft are shown on the σ'_r - τ plane at various pile depths. These paths are characterised by a first reduction in the radial stress followed by a monotonic increase toward the failure line, of slope δ_{cv}, due to the soil dilation. This pattern is in close agreement with the main experimental findings on the subject (e.g. Lehane et al., 1993).

3.3. Comparison with CPT-based predictive methods

The results are compared with those obtained by the load-transfer curve method in the formulation recently proposed by Lehane et al. (2020b). The mobilised shaft resistance is given as:

$$\frac{\tau}{\tau_f} = \left(\frac{G}{\tau_f}\right)\left(\frac{w}{2D}\right)\left[1 - \frac{w}{2 \cdot D \cdot \frac{q_c^{0.5}\sigma'^{0.25}_{v0}}{A p_a^{0.75}}}\right] \tag{10}$$

where G is the operational shear modulus and $A = 625$ for piles loaded in tension and the ultimate shaft resistance, τ_f, is calculated with the unified CPT-method as:

$$\tau_f = f(\sigma'_{ri} + \Delta\sigma'_r)tan(\delta) \tag{11}$$

where $f = 0.75$, and $\delta = 29°$. The initial radial stress σ'_{ri} is as per Eq. (2), with the PLR function of the pile thickness and:

$$\Delta\sigma'_r = \frac{q_c}{10}\left(\frac{q_c}{\sigma'_{v0}}\right)^{-0.33}\frac{d_{cpt}}{D} \tag{12}$$

where d_{cpt} is the cone diameter. The method is implemented in a one-dimensional model using a ten elements discretisation and suitably averaging the experimental profile of q_c (Fig. 4). The results, displayed in Fig. 7 with grey lines, predict a slightly stiffer response and higher capacity with respect to the experimental.

4. Concluding remarks

The paper presents a continuum approach to predict the behaviour of steel piles driven in a uniform sand deposit and subjected to a drained axial pull-out. It requires CPT data and interface laboratory tests to be implemented. The implementation is simple and the computational cost is low with a simulation running in about thirty minutes, using a standard workstation (Intel Xeon E3-1240 v5 CPU @ 3.50 GHz, 16 GB RAM).

The modelling approach was applied to model the results of laboratory technical-scale tests and showed accuracy in reproducing the entire load–displacement curve of three piles of different diameters, slenderness and thickness. Both service and ultimate conditions were successfully predicted. The progressive mobilisation of the shear stress along the pile and the stress paths also appeared to be correctly captured and consistent with the relevant experimental literature.

The good performance observed relatively to the considered testing campaign is partly ascribable to the choice of

the empirical correlations, especially suitable for piles installed in a homogenous commercial clean silica sand and the direct implementation of interface test data. This offers a possible explanation to the scatter observed between the experimental data and the prediction of the latest CPT-based load-transfer method, which was based on a rich database of instrumented piles installed in natural deposits. These characteristics allow the CPT-based method to be implemented with confidence for pile design at offshore sites, but it is not easily extendable to encompass the considered laboratory conditions.

Conversely, the approach proposed in this work can be a strong support in comparing results from laboratory tests on small- to large-scale piles, since it uses empirical correlations calibrated on artificial deposits and it models the whole pile response until failure by adopting specific soil and interface properties. A broader involvement of data from pile tests and steel-sand interfaces would be required to adequately assess the approach robustness. Therefore, at this stage the method might be used as a support of CPT-based methods, eventually adding information to other characteristics of the monotonic response of axially loaded piles than the ultimate capacity.

Acknowledgement

This work forms part of the activities of the project SEAFLOWER, which has received funding from the European Union's Horizon 2020 research and innovation programme, under the Marie Skłodowska-Curie grant agreement No 891826.

References

ABAQUS, 2014. Version 6.14 User's Manual, Dassault Systèmes Simulia Corp.; Providence, RI, USA.

Broere, W., Van Tol, A.F., 2006. Modelling the bearing capacity of displacement piles in sand. Proc. Inst. Civ. Engineers Geotech. Eng. 159, 195–206.

Ciantia, M.O., O'Sullivan, C., Jardine, R.J., 2019. Pile penetration in crushable soils: insights from micromechanical modelling. In: Proc. of the XVII ECSMGE-2019. Reykjavik, Iceland, pp. 298-317.

De Gennaro, V., Frank, R., 2002. Elasto-plastic analysis of the interface behaviour between granular media and structure. Comput. Geotech. 29, 547–572.

De Nicola, A., Randolph, M.F., 1993. Tensile and compressive shaft capacity of piles in sand. J. Geotech. Eng. 119, 1952–1973.

DeJong, J.T., White, D.J., Randolph, M.F., 2006. Microscale observation and modeling of soil-structure interface behavior using particle image velocimetry. Soils Found. 46, 15–28.

Foglia, A., Abdel-Rahman, K., Wisotzki, E., Quiroz, T., Achmus, M., 2021. Large-scale model tests of a single pile and two-pile groups for an offshore platform in sand. Can. Geotech. J. 58, 1825–1838.

Heins, E., Grabe, J., 2017. Class-A-prediction of lateral pile deformation with respect to vibratory and impact pile driving. Comput. Geotech. 86, 108–119.

Hu, Q., Han, F., Prezzi, M., Salgado, R., Zhao, M., 2022. Finite-element analysis of the lateral load response of monopiles in layered sand. J. Geotech. Geoenvironmental Eng. 148, 1–15.

Jamiolkowski, M., Lo Presti, D.C.F., Manassero, M., 2003. Evaluation of relative density and shear strength of sands from CPT and DMT. The SoilBehav. Soft Gr. Constr. 201–238.

Jardine, R.J., Overy, R.F., Chow, F.C., 1998. Axial capacity of offshore piles in dense north sea sands. J. Geotech. Geoenvironmental Eng. 124, 171–178.

Kulhawy, F.H., Mayne, P.W., 1990. Manual on estimating Soil properties for foundation design. Ithaca (NY, USA).

Lehane, B., Jardine, R.J., Bond, A.J., Frank, R., 1993. Mechanisms of shaft friction in sand from instrumented pile tests. J. Geotech. Engrg. 119 (1), 19–35.

Lehane, B.M., Li, L., Bittar, E.J., 2020b. Cone penetration test-based load-transfer formulations for driven piles in sand. Geotech. Lett. 10, 568–574.

Lehane, B., Liu, Z., Bittar, E., Nadim, F., Lacasse, S., Jardine, R., Carotenuto, P., Rattley, M., Jeanjean, P., Gavin, K., Gilbert, R., Bergan-Haavik, J., Morgan, N., 2020a. A new unified CPT-based axial pile capacity design method for driven piles in sand. Travel Behav. Soc. 20, 331–347.

Mentani, A., Govoni, L., Bourrier, F., 2022. The use of CPT based metamodels to predict the performance of offshore anchor piles. In: Cone Penetration Testing 2022. CRC Press, London, pp. 1016–1022. https://doi.org/10.1201/9781003308829-153.

Mentani, A., Govoni, L., Bourrier, F., Zabatta, R., 2023. Metamodelling of the load-displacement response of offshore piles in sand. Comput. Geotech. 159 105490.

Randolph, M.F., Gourvenec, S., 2011. Offshore Geotechnical Engineering, first ed. CRC Press.

Robertson, P.K., 2009. Interpretation of cone penetration tests-a unified approach. Can. Geotech. J. 46, 1337–1355.

Schmoor, K.A., Achmus, M., Foglia, A., Wefer, M., 2018. Reliability of design approaches for axially loaded offshore piles and its consequences with respect to the North Sea. J. Rock Mech. Geotech. Eng. 10, 1112–1121.

Staubach, P., Machaček, J., Wichtmann, T., 2022. Novel approach to apply existing constitutive soil models to the modelling of interfaces. Int. J. Numer. Anal. Methods Geomech. 46, 1241–1271.

Tovar-Valencia, R.D., Galvis-Castro, A., Salgado, R., Prezzi, M., 2018. Effect of surface roughness on the shaft resistance of displacement model piles in sand. J. Geotech. Geoenviron. Eng., 144

Wakai, A., Gose, S., Ugai, K., 1999. 3-D elasto-plastic finite element analyses of pile foundations subjected to lateral loading. Soils Found. 39, 97–111.

White, D.J., Lehane, B.M., 2004. Friction fatigue on displacement piles in sand. Géotechnique 54, 645–658.

Zhang, Q., Feng, R., Yu, Y., Liu, S., Qian, J., 2019. Simplified approach for prediction of nonlinear response of bored pile embedded in sand. Soils Found. 59, 1562–1578.